Mineralium Deposita (2001) 36: 58–71

ARTICLE

Hassan M. Helmy · Aberra Mogessie

Gabbro Akarem, Eastern Desert, Egypt: Cu–Ni–PGE mineralization in a concentrically zoned mafic–ultramafic complex

Received: 3 November 1999 / Accepted: 29 July 2000

Abstract The Gabbro Akarem (Late Precambrian) intrusion is concentrically zoned with a dunite core surrounded by lherzolite–clinopyroxenite enveloped by olivine–plagioclase hornblendite and plagioclase hornblendite. Cu–Ni–PGE mineralization is closely associated with peridotite, especially in the inner, olivine-rich core (dunite pipes) where net-textured and massive sulfides (pyrrhotite, pentlandite, chalcopyrite) are found in association with Al–Mg-rich spinel and Cr-magnetite. Primary magmatic textures are well preserved; however, deformation and mobilization due to shearing are locally observed. Platinum-group minerals (PGM) documented from the deposit are: merenskyite ($PdTe_2$) and michenerite (PdTeBi), as well as palladian bismuthian melonite (Ni,Pd) $(Te,Bi)_2$. These minerals occur in intimate association with hessite (Ag_2Te) and electrum ($Au_{0.65}Ag_{0.31}Bi_{0.04}$) in two distinct textural positions: (1) as inclusions in pyrrhotite, pentlandite, and rarely chalcopyrite and (2) at sulfide–silicate grain boundaries and on microfractures in base-metal sulfides (BMS) and olivine associated with serpentine and secondary magnetite. Textural features suggest that PGM were exsolved from monosulfide solid solution over a wide range of temperatures. Late-stage, low-temperature hydrothermal solutions led to redistribution of PGE. Mineralized samples show Ni/Cu ratios ranging from 0.2 to 2 with an average of 1.0. The (Pt + Pd + Rh)/(Os + Ir + Ru) ratio is generally >6 in most samples, and Os, Ru, and Ir are below the detection limit (2 ppb). The PGE contents show positive correlation with S only at low sulfur contents. The PGE patterns of Gabbro Akarem are similar to those of Alaskan-type deposits. Compared with stratiform deposits, Gabbro Akarem is depleted in PGE. The consistently low PGE contents of the mineralization and their uniform distribution in the ultramafic rocks despite the high sulfur content of the rock is attributed to rapid crystallization of sulfides in a highly dynamic environment.

Editorial handling: O. A. R. Thalhammer

H. M. Helmy (✉)
Geology Department,
Faculty of Science,
Minia University,
61111-Minia, Egypt
e-mail: rumenia@rusys.eg.net; Fax: +20-86-342601

A. Mogessie
Institute of Mineralogy and Petrology,
Karl-Franzens-University,
Universitätsplatz 2, 8010 Graz, Austria

Introduction

Concentrically zoned (Alaskan-type) complexes are relatively small intrusions, elliptical in shape, and composed of a dunite core surrounded by olivine clinopyroxenite, magnetite–hornblende clinopyroxenite, and gabbro (e.g., Taylor 1967; Cabri 1981; Nixon et al. 1990; Fershtater et al. 1997). This type of intrusion is common in southeastern Alaska, Russia, Australia, Canada, Colombia, and Venezuela, ranging in age from Cambrian (Serpentine Hill Complex, Canada, Brown et al. 1988) to Early Miocene (Alto Condoto, Colombia, Tistl 1994). Most of the Alaskan-type complexes are located along major structures and their petrogenesis is still a matter of debate (Garuti et al. 1997; Efimov 1998). The details of the emplacement histories of concentrically zoned complexes vary depending on locality. However, there is general agreement that the intrusion of a hot, ultramafic mush was a key factor in their evolution (Findlay 1969; Irvine 1974). The emplacement of concentrically zoned complexes into shallow crustal levels seems to be controlled by large transverse movements along major lineaments during crustal extension and subsequent ascent from a mantle plume (Tistl and Salazar 1993; Chashchin 1998) in a dynamic environment. Helmy and El Mahallawi (1999) propose that the rapid rise of a hydrous mantle magma along major fracture zones accompanied by

internal circulation and strong vertical stretching, up to the center of the rising magmatic body, led to the concentric zoning of these complexes.

Platinum-group element mineralizations have been described in a number of these complexes where the dunite cores contain native platinum or Pt–Fe and Pt–Ir alloys commonly associated with chromitite (e.g., Razin 1976). In the majority of these complexes, the Pt–Fe and Pt–Ir alloys are not associated with primary magmatic base-metal sulfides (Cabri 1981) but occur as inclusions in chromitites. Cu–Ni–PGE mineralizations are not common in concentrically zoned complexes; only one example was described from the Salt Chuck intrusion, Prince of Wales Island (Loney and Himmelberg 1992).

The Gabbro Akarem Cu–Ni deposit was discovered during a regional geochemical survey project in the South Eastern Desert of Egypt (Bugrov and Shalaby 1973). Disseminated and massive sulfide mineralization occurs in a dike-like mafic–ultramafic intrusion of Late Precambrian age. Plagioclase hornblendite, olivine–plagioclase hornblendite, and peridotite, in decreasing order of abundance, are the main rock units. Geological mapping, geochemical and geophysical exploration, and diamond drilling (15 drill holes with a total of 1,888 m) were conducted by the geologists of the Aswan Mineral Survey Project (1973–1974, Carter 1975; Shabaan et al. 1977). The Cu–Ni mineralization is closely associated with the peridotites. Ore reserves are estimated to be 700,000 tonnes containing 0.95% combined Ni and Cu (Carter 1975). No mining activities have been initiated so far. Relevant studies on the mineralogy and geochemistry of the Gabbro Akarem mineralization are those by Hafez and Abdel-Kader (1982), Rasmy (1982), and Niazy et al. (1985). More recently, Sharara et al. (1999) have studied the mineralogy, mineral chemistry, and isotope geochemistry of the deposit. They concluded that Pd, Rh, and Ir are present within the Fe–Ni–Cu sulfides, while Au and Pt form discrete mineral grains; no platinum-group minerals were described. PGE distributions are explained by fractional crystallization of a monosulfide solid solution from parental sulfide liquid.

The Gabbro Akarem intrusion is elliptical in shape and shows concentric zoning with a dunite core enveloped by lherzolites, pyroxenites, olivine–plagioclase hornblendite, and plagioclase hornblendite. In addition to the concentric zoning and elliptical shape, the Gabbro Akarem rocks are dominated by olivine, clinopyroxene, hornblende, and Fe^{3+}-rich spinel (Helmy and El Mahallawi 1999), features which are identical to Alaskan-type complexes (e.g., Taylor 1967; Mues-Schumacher et al. 1996; Efimov 1998). The aim of this paper is to: (1) describe the geology of the Cu–Ni–PGE deposit; (2) study the mineralogy of the mineralization with special emphasis on PGE mineralogy; (3) study the geochemistry of ore and rock samples; and (4) relate the genesis of the mineralization to the magmatic history of the intrusion.

Geologic setting

The Gabbro Akarem area is located 130 km east of Aswan in the South Eastern Desert of Egypt (Fig. 1). This region is part of the Proterozoic Shield cropping out east of the Nile River, and comprises metasediments, mafic to intermediate metavolcanics, granitoids, and abundant ultramafic rocks. Pelitic and semi-pelitic metasediments (metamorphosed under amphibolite and greenschist facies conditions) are known from different areas. They are considered to be the oldest rock units in the Eastern Desert of Egypt (see also Hassan and Hashad 1990). The metavolcanics are either pillow basalts as a member of the ophiolitic association or andesitic rocks with island arc chemical characteristics (Stern 1981). Granites and granitoids constitute an important rock group that covers about 40,000 km^2 of the shield rocks in Egypt.

Mafic–ultramafic rocks cover about 5% of the South Eastern Desert (Dixon 1979). These rocks are either tectonically emplaced (ophiolitic) or magmatically intruded. Intrusive mafic–ultramafic rocks are minor and are known from a few localities in the South Eastern Desert (e.g., Zabargad island, Bonatti et al. 1981; Gebel Dahanib, Takla 1971; Dixon 1979, 1981a, b; Abu Hammamid, Hafez et al. 1991; Genina Gharbia, Khudeir 1995; and Gabbro Akarem, Carter 1975; Khudeir et al. 1996). The Zabargad peridotite is considered a tectonically uplifted fragment of sub-Red Sea lithosphere (Bonatti et al. 1981). Other complexes are emplaced along major fault zones trending ENE (Fig. 1; Garson and Krs 1976). Although no absolute ages of the intrusive mafic–ultramafic rocks have been determined, crosscutting relationships suggest that they pre-dated the (G2, 620–580 Ma) calc-alkaline granitoid rocks (Hassan and Hashad 1990). Quartz diorite–granodiorite rocks from the Gebel Dahanib complex (80 km to the southeast of Gabbro Akarem) were emplaced at about 710 Ma (Dixon 1981b).

The Gabbro Akarem mafic–ultramafic intrusion consists of an eastern and western body, 1.5 km apart (Fig. 2). In plan, the size of the western mass is 3 × 0.5 km, formed of plagioclase hornblendite, olivine–plagioclase hornblendite, and peridotite, in decreasing

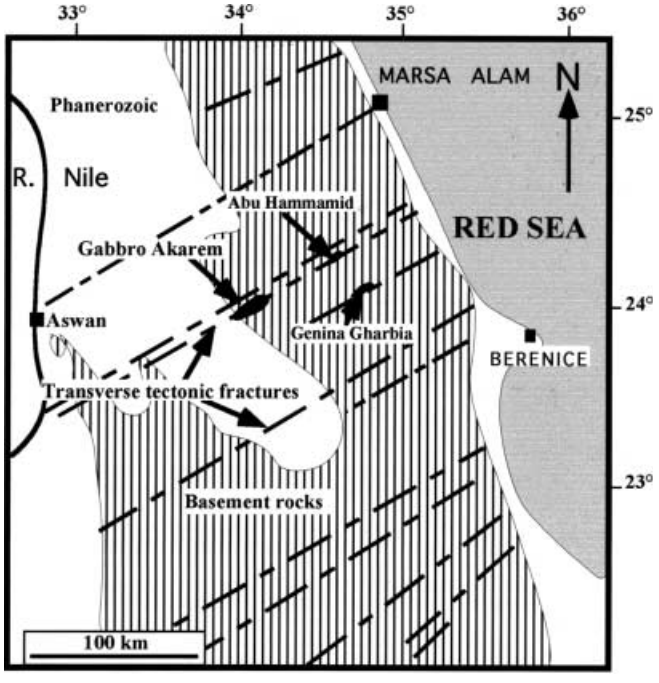

Fig. 1 Location map of the Gabbro Akarem and other concentrically zoned intrusions in the Eastern Desert of Egypt. Deep structures revealed by geophysical studies in the Eastern Desert of Egypt from Garson and Shalaby (1976)

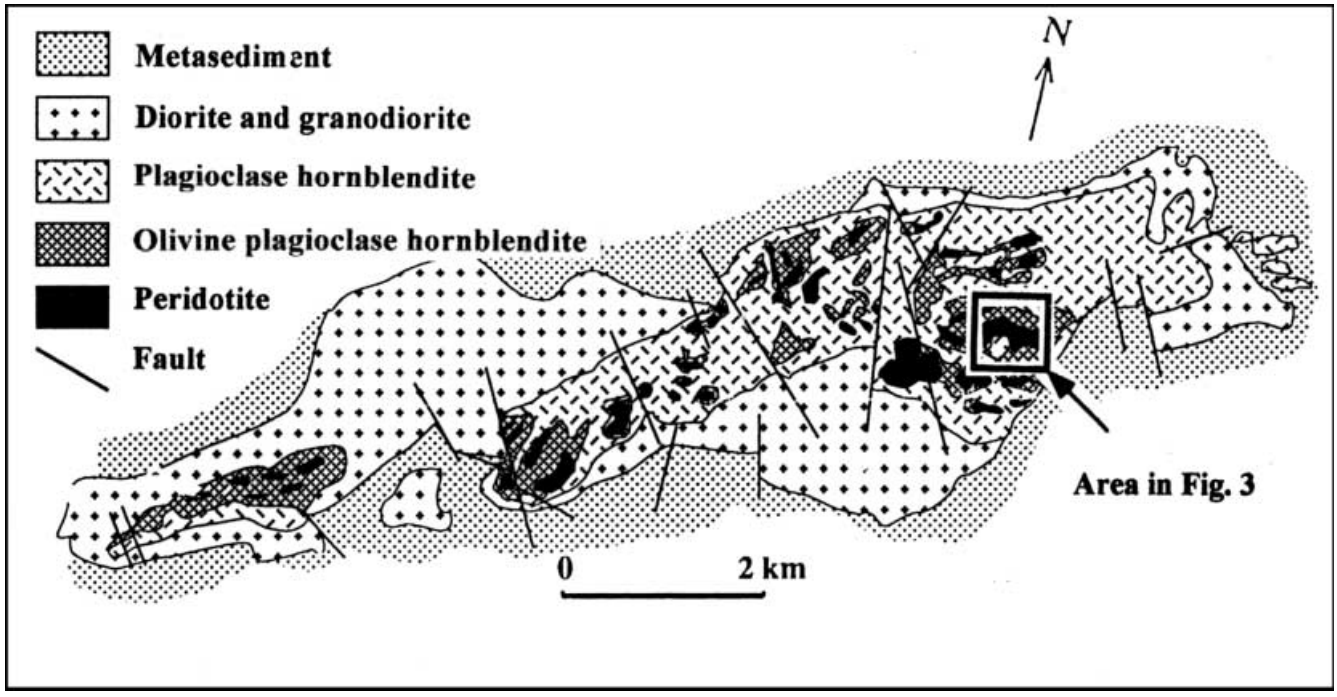

Fig. 2 Geological map of the Gabbro Akarem area, Eastern Desert, Egypt (Carter 1975)

order of abundance. The eastern body measures approximately 7×2 km. Plagioclase hornblendite is the major rock type and forms the outer margins of the intrusion in contact with metasediments. Olivine–plagioclase hornblendite is the second most abundant rock type and is located at the contact between plagioclase hornblendite and lherzolite. The peridotite bodies are present in the inner part of the intrusion (Figs. 2, 3) where they are oriented and elongated in a NE–SW direction, following the regional trend of the intrusion. In the eastern part of the intrusion, the peridotite bodies have highly mineralized cores ($>30\%$ volume sulfides) and less mineralized margins ($<10\%$ sulfides). During tectonism, the intrusion was dissected by a large number of normal faults (Carter 1975), which were accompanied by brecciation and lateral displacement. One of these faults has displaced the intrusion into two bodies (Fig. 2). Small-scale shearing is recognized on the surface and in drill cores in the form of serpentinization of olivine and development of secondary sulfide veinlets.

It is known from geophysical data (Shabaan et al. 1977) and diamond drilling that the contact between the mafic–ultramafic intrusion and older metasediments is steep, indicating faulted contacts. Plagioclase hornblendite and pyroxenite dikes from the main body locally intrude tens of meters into the country rocks resulting in garnetiferous metasediments along a narrow zone of contact metamorphism (Carter 1975). A reinterpretation of the magnetic anomalies presented by Shabaan et al. (1977) showed that the mineralized dunite and the surrounding lherzolites extend almost vertically downward to at least 500 m (Helmy and Abu Heleka, unpublished). Because of the vertical extension and the rounded to subrounded sections of the mineralized dunite, they are called dunite pipes throughout this paper.

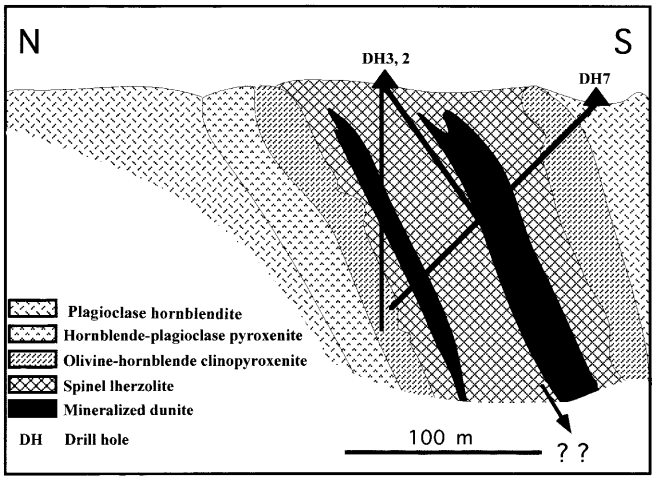

Fig. 3 Vertical cross section of the mineralized dunite pipes from Gabbro Akarem area (data from Carter 1975, modified from Garson and Shalaby 1976)

Analytical techniques

Samples for this study were collected from surface exposures from the eastern body of the intrusion. Additional samples were collected from 15 drill cores with a total length of 1.888 m (at the Geological Survey of Egypt) that intersect variably mineralized rocks and are considered representative of the different mineralization types. Petrographic work as well as silicate, sulfide, and platinum-group mineral analyses were performed on 43 polished thin sections, the latter using a Jeol JSM-6310 scanning electron microprobe with attached energy dispersive system (EDX) and Microspec wavelength dispersive system (WDX) at the Institute of Mineralogy and Petrology, Karl-Franzens University of Graz, Austria. The accelerating voltage was 20 kV for the analysis of sulfides and PGM, and 15 kV for silicates at a probe current of 5 nA. Silicate standards were adularia for Si, K, and Al, garnet for Fe, Mg, and Mn, titanite for Ca and Ti, chromite for Cr, and jadeite for Na. Standards for sulfides and PGM were chalcopyrite for Cu, pyrite for S and Fe, native Ni, and Co, tellurobismuthite (Bi_2Te_3) for Bi and Te, PdS for Pd, sperrylite ($PtAs_2$) for Pt, and calaverite ($AuTe_2$) for Au and native silver. Nineteen samples were analyzed for PGE and Au by ICP-MS (nickel sulfide digest), Ag, Ni, Co, and Cu by Flame-AAS (triple acid digest), and for S by ICP-OES (triple acid digest) by Genalysis, Australia. The detection limit of PGEs was 2 ppb for Ir, Os, and Ru and 1 ppb for Pt, Pd, and Rh, respectively.

Petrography

The mineralogy and petrology of the Gabbro Akarem intrusion was recently studied by El Mahallawi and Helmy (1997). The intrusion is composed of plagioclase hornblendite (60% by volume), olivine–plagioclase hornblendite (20% by volume), hornblende–plagioclase pyroxenite, olivine–hornblende clinopyroxenite, lherzolite, and dunite (about 17% by volume). Coarse-grained and pegmatitic textures are common in the whole intrusion, but they are more abundant in hornblende-bearing pyroxenites. Minor serpentinization of olivine occurred in the dunite core and along shear zones, but most other rocks of the intrusion are fresh.

The plagioclase hornblendite is a medium-grained rock composed of hornblende (up to 55 modal proportion), plagioclase (up to 35%) and orthopyroxene (2–5 %). Small-scale layering defined by amphibole and plagioclase is locally observed. Large hornblende crystals commonly contain unoriented small elongated inclusions of plagioclase.

The mineralized dunite pipes are enveloped by sulfide-containing ultramafic rocks zoned laterally from inner spinel lherzolite through olivine–hornblende clinopyroxenite to outermost hornblende–plagioclase pyroxenite.

Spinel lherzolite contains 57–62 modal % of olivine, 23–25% orthopyroxene, 9–12% clinopyroxene, chrome spinel (4% modal), and trace hornblende.

Olivine–hornblende clinopyroxenite is a coarse-grained rock and contains mainly clinopyroxene (40 modal %), olivine (32%), orthopyroxene (11%), and hornblende (up to 25%). Olivine and pyroxenes form large (3–4 mm) cumulus crystals. Hornblende forms large euhedral crystals in textural equilibrium with the spinel-bearing assemblage.

Hornblende–plagioclase pyroxenite has a wide range of modal compositions with orthopyroxene (24–31 modal %), olivine (20–35%), clinopyroxene (17–23%), hornblende (15–18%), and plagioclase (9–12%) showing hypidiomorphic texture. The content of sulfides in the different ultramafic rocks varies from 5 to 15 modal %.

In the dunite core, olivine represents >90 modal % of the silicate assemblage with clinopyroxene, hornblende, orthopyroxene, and spinel in a decreasing order of abundance. Intercumulus sulfides constitute up to 70 modal % of the dunite. Tschermakitic and pargasitic hornblende are present as large intercumulus crystals in equilibrium with olivine (Fig. 4A) and as a reaction rim at the contact between olivine and base-metal sulfides. Two types of chrome spinel are identified in the dunite: a dark gray (in reflected light), Al–Mg–Cr-rich variety and a light gray, Fe-rich chromian magnetite. In places, the two types occur together as small inclusions in olivine. Cr-magnetite forms >90 modal % of the total spinel. It is found as individual grains, inclusions in sulfides, and as intercumulus crystals between olivine grains and sulfides (Fig. 4B).

Petrographic observations at Gabbro Akarem indicate early magmatic crystallization of olivine and chrome spinel in the dunite core. In the clinopyroxene–hornblende-rich ultramafic rocks, orthopyroxene, clinopyroxene, and hornblende begin crystallization alongside olivine. Orthopyroxene and hornblende have the longest crystallization history in the intrusion (as indicated by their abundance in both ultramafic and mafic rocks and their wide range of Mg#, Tables 1 and 2). The observed interstitial hornblende in the dunite core most probably indicates crystallization from trapped interstitial melt. Plagioclase crystallized alongside hornblende to form the hornblende–plagioclase pyroxenite and the plagioclase hornblendite.

Fig. 4 **A** Hornblende (*Hbl*) in equilibrium with olivine (*Ol*) from mineralized dunite, *small white crystals* are spinel. Back scattered image, sample GA149. **B** Intercumulus magnetite (*Mag*) and sulfides (pyrrhotite, *Po*) with cumulus olivine (*Ol*). Back scattered image, sample AC157

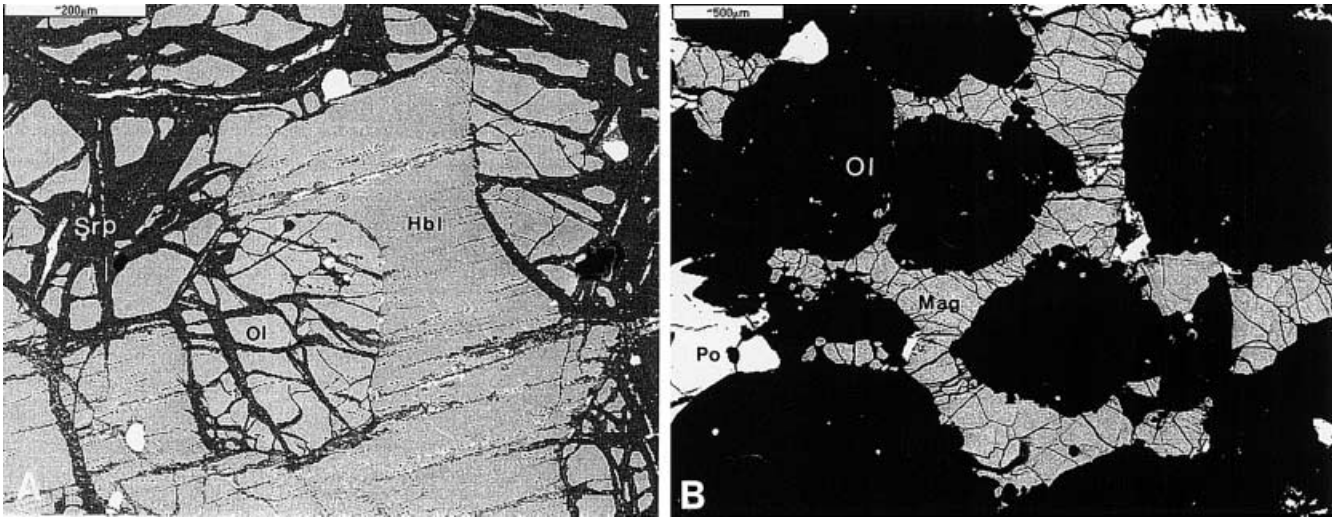

Table 1 Representative electron microprobe analyses of silicates and oxide minerals, Gabbro Akarem area. *Sp lhz* spinel lherzolite, *Plg hnbl* plagioclase hornblendite, *Hbl plg px* hornblende–plagioclase pyroxenite, *Ol hbl cpx* olivine–hornblende clinopyroxenite, *nd* not determined

	Olivine				Orthopyroxene			Clinopyroxene		Hornblende			Spinel	
	GA159 Sp lhz	GA158 Sp lhz	GAC Dunite	GA138 Plg hnbl	GA145 Hbl plg px	GA155 Dunite	GA145 Hbl plg px	GA159 Dunite	GA159 Dunite	GA126 Plg hnbl	GA143 Ol hbl cpx	GA159 Dunite	GA153 Dunite	GA153 Dunite
SiO_2	38.25	39.34	39.99	53.14	53.94	55.45	51.48	52.05	53.19	43.61	43.58	44.48	0.00	0.00
TiO_2	0.00	0.00	0.00	0.13	0.26	0.06	0.31	0.39	0.21	1.15	1.17	1.33	0.18	0.12
Al_2O_3	0.00	0.00	0.00	1.25	2.95	1.95	3.33	3.97	2.52	13.63	12.52	12.35	28.18	1.69
Cr_2O_3	0.00	0.00	0.00	0.15	0.23	0.29	0.47	1.01	1.09	0.31	1.02	1.38	26.59	9.80
FeO	19.39	15.21	12.82	22.99	12.18	10.28	4.42	3.96	5.52	11.53	8.16	6.73	25.44	30.14
Fe_2O_3	nd	nd	nd	nd	nd	nd	nd	nd	nd	nd	nd	nd	11.74	56.14
MnO	0.36	0.35	0.31	0.59	0.26	0.38	0.17	0.14	0.19	0.19	0.12	0.12	0.61	0.50
MgO	41.35	44.81	46.09	22.76	27.86	30.11	15.57	15.13	18.15	13.76	15.57	17.79	6.68	0.92
CaO	0.00	0.00	0.00	0.87	1.23	0.56	23.17	23.45	20.12	11.06	12.77	12.25	0.00	0.00
Na_2O	0.00	0.00	0.00	0.00	0.08	0.00	0.31	0.56	0.27	2.39	1.95	2.09	0.00	0.00
K_2O	0.00	0.00	0.00	0.00	0.00	0.00	0.00	0.00	0.00	0.28	0.61	0.61	0.00	0.00
$\sum$	99.35	99.71	99.21	101.88	98.99	99.08	99.23	100.66	101.26	97.91	97.47	99.13	99.42	99.32
O	4.000	4.000	4.000	6.000	6.000	6.000	6.000	6.000	6.000	23.000	23.000	23.000	32.000	32.000
Si	0.989	0.993	1.002	1.962	1.937	1.967	1.906	1.898	1.922	6.346	6.330	6.307	0.000	0.000
Ti	0.000	0.000	0.000	0.004	0.007	0.002	0.009	0.011	0.006	0.126	0.128	0.142	0.030	0.030
Al	0.000	0.000	0.000	0.054	0.125	0.082	0.145	0.171	0.106	2.337	2.143	2.064	8.390	0.610
Cr	0.000	0.000	0.000	0.004	0.007	0.008	0.014	0.029	0.031	0.036	0.117	0.155	5.310	2.360
Fe^{2+}	0.419	0.321	0.269	0.710	0.366	0.305	0.137	0.121	0.167	1.403	0.991	0.798	5.380	7.670
Fe^{3+}	–	–	–	–	–	–	–	–	–	–	–	–	2.230	12.860
Mn	0.008	0.007	0.007	0.018	0.008	0.011	0.005	0.004	0.006	0.024	0.015	0.015	0.130	0.130
Mg	1.594	1.686	1.729	1.245	1.491	1.592	0.859	0.822	0.977	2.984	3.371	3.760	2.520	0.870
Ca	0.000	0.000	0.000	0.034	0.047	0.021	0.919	0.916	0.779	1.724	1.987	1.861	0.000	0.000
Na	0.000	0.000	0.000	0.000	0.006	0.000	0.022	0.040	0.019	0.674	0.549	0.574	0.000	0.000
K	0.000	0.000	0.000	0.000	0.000	0.000	0.000	0.000	0.000	0.052	0.113	0.111	0.000	0.000
$\sum$ Cations	3.010	3.007	3.007	4.031	3.993	3.987	4.017	4.011	4.013	15.705	15.744	15.785	24.990	24.530
Mg#	0.792	0.840	0.865	0.638	0.803	0.839	0.863	0.872	0.854	0.680	0.773	0.825	0.390	0.050

Mineral chemistry

A summary of the mineral chemistry data and representative electron microprobe analyses of different mineral phases are presented in Tables 1 and 2. With increasing modal proportion of clinopyroxene, hornblende, and plagioclase, the Mg# ($Mg/Mg + Fe^{2+}$) of olivine decreases from 0.87 mol% in dunite through 0.81 mol% in hornblende–plagioclase pyroxenite to 0.69 in olivine–plagioclase hornblendite. Orthopyroxene shows the widest range of composition with Mg# values ranging from 0.59 in plagioclase hornblendite to 0.85 in dunite. Clinopyroxenes are represented by diopside and magnesian augite with Mg# values ranging from 0.83 to 0.89. High Cr_2O_3 (0.37–1.34 wt%) and Al_2O_3 (2.52–4.18 wt%) values were recorded in the clinopyroxenes. The Mg# of hornblende ranges from 0.62 in plagioclase hornblendite to 0.88 in the dunite. Hornblende in dunite is enriched in Cr_2O_3 (0.76–1.90 wt%), and a positive correlation between Cr and Mg# is observed. High TiO_2 contents (0.8–2.6 wt%) are recorded in hornblende from the plagioclase hornblendite. The An content of plagioclase increases from 85% in plagioclase hornblendite to 88% in lherzolite.

The Al–Mg-rich spinel reveals a wide range of Al_2O_3 (15.7–42.9 wt%), Cr_2O_3 (17.7–29.1 wt%), and MgO (4.1–12.7 wt%) contents. A wide range of calculated Fe^{3+}/Fe^{2+} (0.3–0.7) and Cr# (Cr/Cr + Al, 0.2–0.7) ratios is observed. Cr-magnetite contains Cr_2O_3 within the range of 4.7–18.9 wt%, whereas Al_2O_3 and MgO contents vary from 0.3 to 4.4 wt% and 0.6 to 1.9 wt%, respectively. The Fe^{3+}/Fe^{2+} and Cr# ratios in the Cr-magnetite are within the range of 1.4–1.9 and 0.4–0.9, respectively. The MnO contents in both types of spinel are similar (i.e., <0.8 wt%). Figure 5 compares the spinel compositions of Gabbro Akarem with spinels from other settings. Although not plotting within the field of typical southeast Alaskan-type complexes, spinels from Gabbro Akarem are comparable with those from the Tulameen complex (typical Alaskan-type; Nixon et al. 1990) and the Bear Mountain complex (argued to be an Alaskan-type complex; Snoke et al. 1981).

Sulfide mineralization

General features of the ore

Variable amounts of Fe, Ni, Cu, and Co sulfides (mainly pyrrhotite, pentlandite, and chalcopyrite) are observed in all rock units. Small amounts (<0.3 modal %) are encountered in plagioclase hornblendite and olivine–plagioclase hornblendite; however, higher values

Table 2 Summary of the mineralogical data of different rocks from Gabbro Akarem. Modal % determined by point counting; Mg# = Mg/(Mg + Fe) and Cr# = Cr/(Cr + Al); *n* number of samples

Rock type	Olivine		Orthopyroxene		Clinopyroxene		Amphibole		Plagioclase		Spinel		Sulfides
	Modal %	Mg#	Modal %	Mg#	Modal %	Mg#	Modal %	Mg#	Modal %	An content	Modal %	Cr#	Modal %
Plagioclase hornblendite $n=5$	–	–	2–7	0.59–0.66	–	–	48–59	0.62–0.66	32–38	79–83	< 1	–	< 0.3
Ol plg hornblendite $n=3$	3–5	0.67–0.69	4–9	0.64–0.72	–	–	49–56	0.64–0.69	30–36	81–83	2	–	0.5–5
Hbl plg pyroxenite $n=5$	20–35	0.79–0.81	24–31	0.74–0.76	17–23	–	15–18	0.67–0.75	8–11	85–88	2	–	7–9
Ol hbl clinopyroxenite $n=6$	28–33	0.82–0.84	8–13	0.78–0.79	35–44	0.85–0.92	4–12	0.74–0.82	< 3	–	2	–	5–8
Sp lherzolite $n=4$	57–62	0.85–0.86	23–25	0.79–0.82	9–12	0.87–0.93	4–11	0.78–0.85	< 2	0.88	2	–	5–11
Dunite $n=8$	91–95	0.84–0.87	3–5	0.80–0.85	3–4	0.89–0.96	3–6	0.81–0.88	< 1	–	3	0.75–0.90	15–70

(< 3 modal %) are recorded close to the contacts of these rocks with peridotite. Thin zones, a few meters wide, containing up to 5 modal % sulfides are developed along fracture zones (Carter 1975) in plagioclase hornblendite, and even higher sulfide contents are found in fracture zones in the olivine–plagioclase hornblendite.

In the ultramafic rocks, sulfides normally amount to more than 5 modal %, and correlate in abundance with increasing modal proportion of olivine. In the dunite, sulfides locally form massive pods up to 15 cm thick. However, the massive ore represents a small fraction of the total mineralization. Two pipe-like bodies of mineralized dunite were encountered in drillcores 2, 3, and 7; these are termed the hangingwall and footwall zones (Carter 1975; Fig. 3). The hangingwall zone is a vertical body with elliptical plane section. This body has a strike length of 300 m and maximum width of 80 m. The footwall zone has a strike extent of about 75 m and 5 m thickness, as indicated by drill cores 3 and 7. At the surface, weathered sulfides form gossan zones up to 3 m thick and are traced for about 250 m adjacent to peridotite–plagioclase hornblendite contacts (Bugrov and Shalaby 1973).

In summary, the sulfide mineralization is mainly associated with the ultramafic rocks with local enrichment in the mafic rocks. Post-intrusion shearing resulted in minor remobilization and redistribution of sulfides.

Sulfide mineralogy and chemistry

The main sulfide minerals noted above occur with lesser amounts of cubanite and pyrite. Mackinawite, Cr-valleriite, and marcasite are present as secondary minerals. Although sulfides in plagioclase hornblendite and olivine–plagioclase hornblendite are normally present in amounts up to 0.3%, they occur in similar modal proportions to those of highly sulfidic peridotites with pyrrhotite≫pentlandite > chalcopyrite. Pentlandite occurs as fine, flame-like bodies in pyrrhotite while chalcopyrite forms small grains at the outer margin of pyrrhotite. Sulfides (normally < 40 μm in diameter) occur as inclusions in hornblende and interstitial to silicates.

Sulfides in hornblende–plagioclase pyroxenite and lherzolite are coarse-grained and form small patches interstitial to silicates. Pyrrhotite (60 modal %) forms large masses enclosing pentlandite and chalcopyrite. Pentlandite (20 modal %) frequently occurs close to the center of pyrrhotite grains followed by chalcopyrite at the outer margin. Small anhedral pyrite grains are commonly observed close to chalcopyrite grain margins.

Net-textured and massive sulfides (Fig. 6A) in dunite pipes comprise pyrrhotite, pentlandite, chalcopyrite, cubanite, and pyrite in decreasing order of abundance (see also Sharara et al. 1999). Pyrrhotite forms large (0.5–2 mm) anhedral crystals interstitial to olivine and orthopyroxene; in places, it may contain euhedral inclusions of Cr-magnetite (Fig. 6B). Pentlandite forms

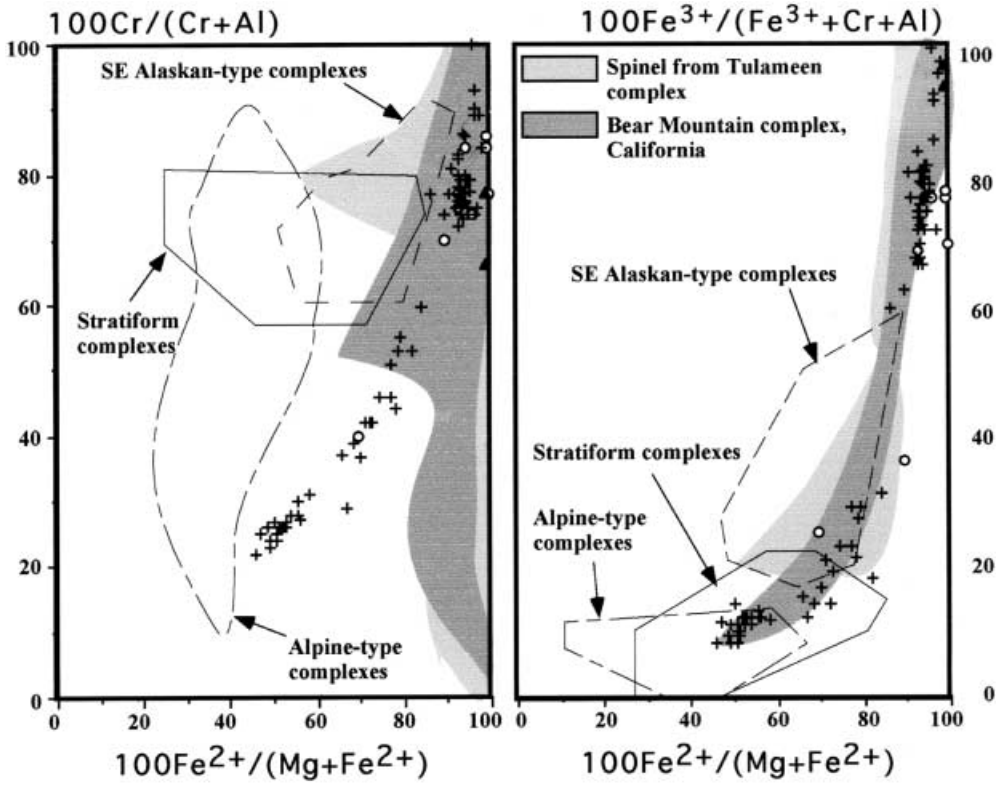

Fig. 5 Variation diagram of $100Cr/(Cr + Al)$ versus $100Fe^{2+}/(Mg + Fe^{2+})$ (*left*) and $100Fe^{3+}/(Fe^{3+} + Cr + Al)$ versus $100Fe^{2+}/(Mg + Fe^{2+})$ (*right*) for spinel from Gabbro Akarem. Fields for Alpine-type peridotites, stratiform intrusions, and southeast Alaskan-type complexes are adapted from Irvine (1967). Fields for Tulameen and Bear Mountain Alaskan-type complexes from Nixon et al. (1990) and Snoke et al. (1981). *Crosses* Spinel from dunite; *open circles* hornblende clinopyroxene-rich ultramafics; *triangles* plagioclase hornblendite

either rounded crystals included in pyrrhotite or veinlets along cracks in pyrrhotite. Exsolution flames (Fig. 6C) of pentlandite occur at grain boundaries of pyrrhotite and along microfractures in pyrrhotite. In places, pentlandite may be replaced by violarite (Fig. 6D) and mackinawite. Chalcopyrite occurs as anhedral grains at the outer margins of pyrrhotite and as veinlets crosscutting massive sulfides and in serpentinized olivine. Pyrite is found in micro shear zones and in secondary serpentine–magnesite veinlets crosscutting massive sulfides.

Pyrrhotite is rather homogeneous in composition with low contents of Ni (0.18–0.28 wt%) and Co (0.11–0.20 wt%). The large pentlandite crystals and vein pentlandite have similar compositions with average Fe/Ni ratio of 1.05 and average Co content of 2.18 wt%. Pentlandite exsolutions in pyrrhotite show a wide range of Fe/Ni ratio (0.99–1.29) and consistently low Co content (average = 1.14 wt%). A Co-rich pentlandite was previously described from Gabbro Akarem (Sideek and El Goresy 1996); however, this type of pentlandite was not found in the studied samples. Mackinawite is Ni-rich (6.0–6.2 wt% Ni), and Cu and Co-poor (< 0.32 wt% Cu, < 0.15 wt% Co).

The PGE content of all sulfides are below the microprobe detection limit (0.05 wt%). Sharara et al. (1999) reported low PGE contents (ppb range) in pyrrhotite, pentlandite, and chalcopyrite. Except for palladium in pentlandite, the PGE contents of sulfide minerals are lower than bulk-rock levels (Sharara et al. 1999).

Platinum-group minerals

The PGM from Gabbro Akarem are palladium bismuthotellurides. No Pt-bearing phases were identified. This association is atypical to PGE mineralization hosted in Alaskan-type complexes. PGM are similar to the PGM assemblage from the metamorphosed Abu Swayel Cu–Ni deposit in the Eastern Desert of Egypt (Helmy et al. 1995). PGM, Pd-bearing melonite, electrum, and hessite occur as minute subhedral to anhedral grains, ranging from 5 to 35 μm. The PGM are most common in the sulfide-rich samples and exhibit the following textures:

1. About 80% of the PGM grains (about 85 grains were located in 15 polished surfaces from the massive ore), enclosed in pyrrhotite (Fig. 7A) and occurring along cracks within pyrrhotite (Fig. 7B), are merenskyite with variable Ni contents (1.4–6.6 wt%, Table 3). Merenskyite rarely occurs as inclusions in pentlandite and chalcopyrite.
2. Merenskyite, michenerite, and Pd-bearing bismuthian melonite associated with hessite occur along cracks within sulfides and at the contact between base-metal sulfides and silicate minerals (Fig. 7C, D). Merenskyite, electrum and hessite grains are also observed in serpentine veinlets crosscutting olivine (Fig. 8A, B).

Merenskyite, the most abundant PGM, forms subhedral crystals which range in size from 7 to 35 μm, and

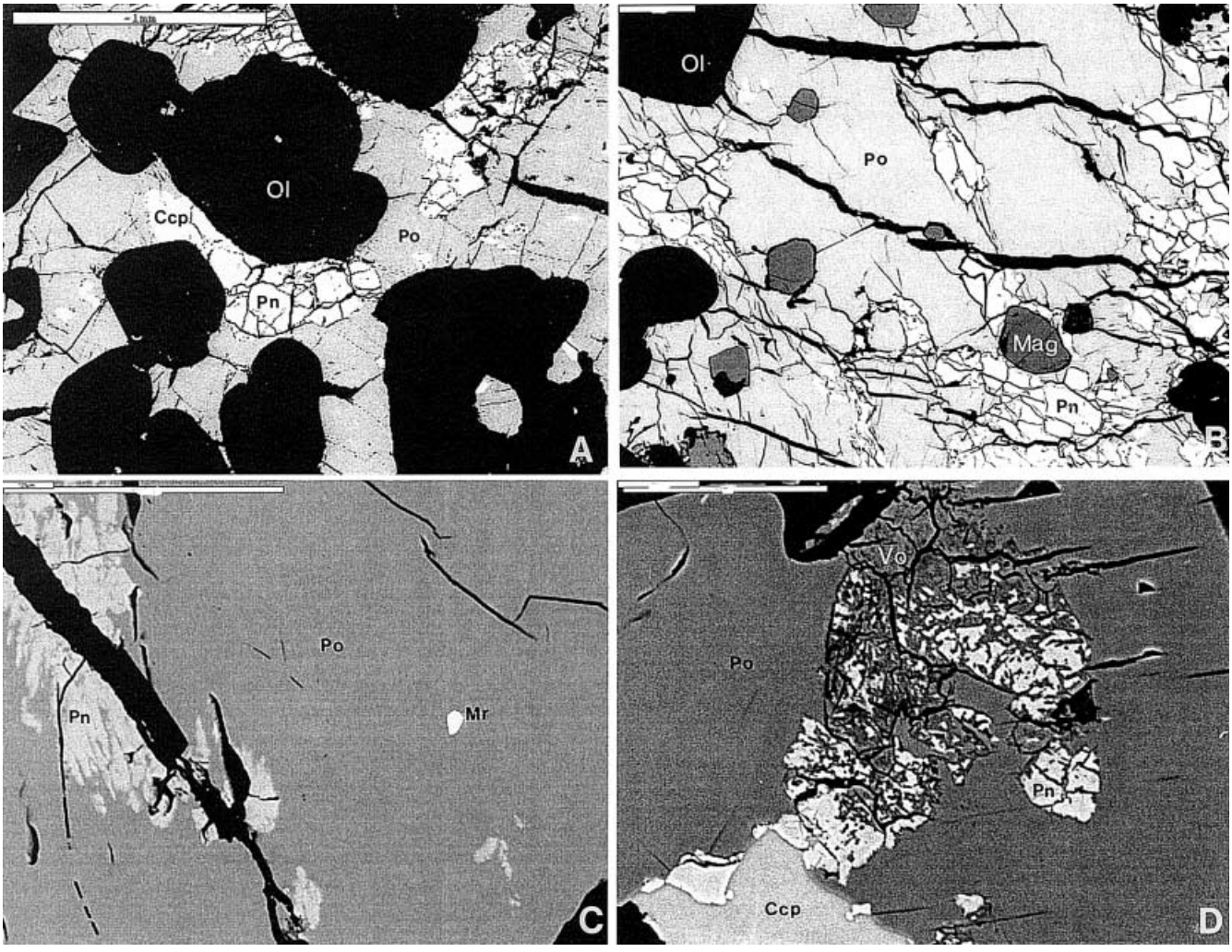

Fig. 6 Back scattered images showing textural features of sulfide ores. **A** Intercumulus sulfides (*Po* pyrrhotite, *Pn* pentlandite, and *Ccp* chalcopyrite) surrounding olivine (*Ol*), sample GA155. **B** Euhedral magnetite included in pyrrhotite (*Po*) and pentlandite (*Pn*), sample GA146, *scale bar* = 200 μm. **C** Exsolutions of pentlandite (*Pn*) along crack in pyrrhotite (*Po*), small merenskyite crystal (*Mr*) is included in pyrrhotite, sample 155, *scale bar* = 100 μm. **D** Pyrrhotite (*Po*) hosting pentlandite (*Pn*) replaced by violarite (*Vo*), sample AC100, *scale bar* = 50 μm

appear white with faintly pinkish tint in reflected light. The analyses show a wide range of substitution of Pd by Ni and Te by Bi. Traces of Ag (< 2.22 wt%), Cu (< 0.27 wt%), and Fe (< 1.17 wt%) were detected. Similar compositional variations in merenskyite were also described from the Abu Swayel deposit (Helmy et al. 1995).

A few grains of michenerite were found at the contact of chalcopyrite with silicates, mainly serpentine and chlorite. The grains range in size from 5 to 17 μm and are commonly associated with hessite. The calculated mineral formula (Table 3) of michenerite is: $Pd_{0.94}Ni_{0.03}Bi_{0.89}Te_{1.14}$.

Pd-bearing bismuthian melonite forms small subhedral crystals (10–20 μm) which are usually associated with hessite. This mineral is generally Pd- (> 9.8 wt%) and Bi- (> 9.2 wt%) rich. In the $PdTe_2$–$PtTe_2$–$NiTe_2$ system, the merenskyite and Pd-bearing bismuthian melonite analyses plot in the Pd-rich portion. Merenskyite and Pd-bearing bismuthian melonite in the Gabbro Akarem rocks represent a solid solution between the Ni end member melonite and the Pd end member merenskyite (Rucklidge 1969; Helmy et al. 1995).

Ore geochemistry

Nineteen rock samples from the Gabbro Akarem intrusion were analyzed for their concentrations of S, Cu, Ni, Co, Zn, Cr, Se, and noble metals (Table 4). The Ni contents (78–589 ppm) in the plagioclase hornblendite and olivine–plagioclase hornblendite are higher than those of Cu (2–65 ppm). Cu exceeds Ni in the spinel lherzolite, olivine–hornblende clinopyroxenite and hornblende–plagioclase pyroxenite. In these rocks, the Ni/Cu ratios range from 0.19 to 0.96 and in one sample (GA158, spinel–lherzolite) only Ni exceeds Cu (Ni/Cu = 1.22). Ni contents in the net-textured and massive sulfide ores of the dunite are generally higher than those

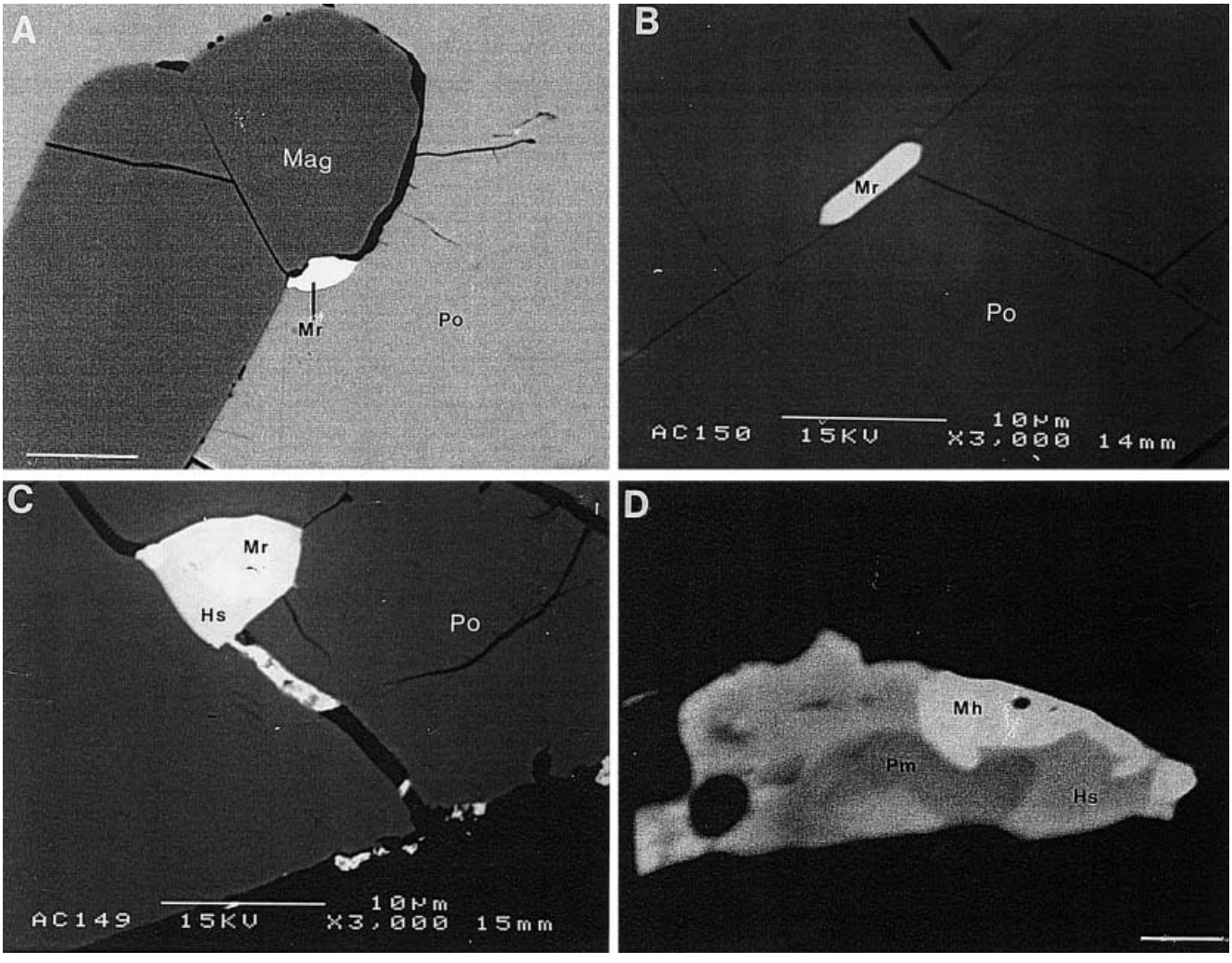

Fig. 7 Back scattered electron images showing textural positions of PGM. **A** Merenskyite (*Mr*) attached to magnetite (*Mag*) included in pyrrhotite (*Po*), sample AC149, *scale bar* = 30 µm. **B** Merenskyite (*Mr*) along micro-cracks in pyrrhotite (*Po*) sample GA151. **C** Merenskyite (*Mr*) and hessite (*Hs*) along crack in pyrrhotite (*Po*), sample GA151. **D** Michenerite (*Mh*), palladian–bismuthian melonite (*Pm*), and hessite (*Hs*) at sulfide–silicate contacts (due to the high magnification and contrast, sulfides and silicates are difficult to recognize in the photo), sample AC146, *scale bar* = 2 µm

of Cu with an average Ni/Cu ratio of 1.27. The average Co content in plagioclase hornblendite, hornblende–plagioclase clinopyroxenite, olivine clinopyroxenite, and spinel lherzolite is 58, 178, 191 and 265 ppm, respectively. A positive correlation between Ni and Co is observed. Low S contents (310–420 ppm) are characteristic of plagioclase hornblendite and olivine–plagioclase hornblendite, as expected from the low modal proportions of sulfides. The S content in pyroxenite and lherzolites ranges from 0.73 to 2.8 wt%, while high values of S (10.1–18.4 wt%) are found in the mineralized dunite pipes.

The main geochemical feature of the Gabbro Akarem Cu–Ni–PGE mineralization is the predominance of Pd over Pt and the depletion of Ir, Os, and Ru in all rock units, as also reported for other PGE mineralization in the Eastern Desert (e.g., Abu Swayel, Helmy and Stumpfl 1995). The (Pd + Pt + Rh)/(Ir + Os + Ru) ratio in samples containing detectable Ir, Os, and Ru is >6.

Figure 9 shows the average chondrite (C1)-normalized PGE patterns of lithologies at Gabbro Akarem and other concentrically zoned complexes. The plagioclase hornblendite is generally depleted in PGE relative to the olivine–hornblende clinopyroxenite (with disseminated ore) and dunite (with net-textured and massive ore). The PGE pattern of net-textured and massive sulfide ore is similar to the PGE pattern of disseminated ore, which may suggest that both were crystallized from the same magma. Although slightly depleted in Pt, Ru, and Os, Gabbro Akarem shows a PGE pattern similar to that of Alaskan-type complexes. Relative to the Salt chuck mineralization, Gabbro Akarem rocks are depleted in Pd and Au.

Discussion

PGE-ore forming processes reflect the complexities in the evolution of the magmatic system as a whole including those in the parental magma source regions and pro-

Table 3 Representative electron microprobe analyses of platinum-group minerals, Pd-bearing bismuthian melonite, electrum, and hessite. Ten analyses, at least, have been obtained for merenskyite, Pd-bearing bismuthian melonite, and electrum, and three analyses for michenerite and hessite

Mineral	Merenskyite							Pd-bearing melonite		Michenerite	Electrum		Hessite
Sample no.	AC149C1	AC149C5	GA155C	GA155	GA155C6	AC148	AC158	AC	AC154	GA146	GA153	GA153C2	AC
Fe	0.60	0.00	0.00	1.17	0.00	0.00	0.42	0.00	0.37	0.00	1.55	1.31	0.66
Cu	0.00	0.27	0.00	0.00	0.00	0.00	0.00	0.08	0.54	0.00	0.09	0.07	0.00
Ni	1.47	4.88	5.12	4.71	5.54	4.80	6.56	9.57	10.15	0.37	0.03	0.04	0.73
Pd	24.63	20.55	19.17	17.46	16.75	19.85	16.47	12.58	10.30	22.71	0.00	0.00	2.73
Ag	2.22	0.00	0.63	0.00	0.00	0.00	0.00	0.85	1.47	0.00	22.14	19.20	53.74
Bi	9.99	17.11	5.80	10.66	7.20	9.54	6.56	10.30	9.88	42.35	3.27	3.94	1.10
Au	0.00	0.00	0.00	0.00	0.00	0.00	0.00	0.00	0.00	0.00	72.14	74.41	0.00
Te	61.20	56.46	70.03	66.69	68.64	67.41	71.07	67.45	67.33	33.21	0.21	0.18	41.28
$\sum$ wt%	100.11	99.25	100.75	100.69	98.13	101.60	101.18	100.83	100.04	98.64	99.43	99.15	99.51
Atomic proportions													
Fe	0.040	0.000	0.000	0.075	0.000	0.000	0.028	0.000	0.024	0.000	0.045	0.040	0.041
Cu	0.000	0.019	0.000	0.000	0.000	0.000	0.000	0.004	0.031	0.000	0.002	0.002	0.000
Ni	0.091	0.309	0.307	0.286	0.342	0.292	0.389	0.563	0.593	0.026	0.000	0.000	0.041
Pd	0.852	0.718	0.635	0.586	0.572	0.665	0.539	0.408	0.333	0.937	0.000	0.000	0.089
Ag	0.077	0.000	0.015	0.000	0.000	0.000	0.000	0.028	0.480	0.000	0.332	0.296	1.704
Bi	0.176	0.305	0.092	0.182	0.127	0.164	0.108	0.169	0.161	0.893	0.260	0.032	0.017
Au	0.000	0.000	0.000	0.000	0.000	0.000	0.000	0.000	0.000	0.000	0.592	0.629	0.000
Te	1.763	1.649	1.938	1.870	1.959	1.879	1.936	1.828	1.810	1.144	0.003	0.002	1.108
$\sum$	2.999	3.000	2.987	2.999	3.000	3.000	3.000	3.000	3.000	3.000	1.000	1.001	3.001

cesses taking place in the magma chamber itself. The petrogenesis of Cu–Ni–PGE mineralization in a magmatic system is largely controlled by the parental magma composition, changes in fS_2, fO_2 and rate of cooling.

At Gabbro Akarem, the net-textured sulfides constitute a small fraction of the total sulfide mineralization. Moreover, sulfides in the marginal (plagioclase hornblendite) rocks are rare. This implies that the parental magma of Gabbro Akarem, like many mantle-derived magmas (McDonough and Sun 1995), was sulfide undersaturated. During the crystallization of the S-undersaturated magma, S, Cu, and Pd partitioned preferentially into the silicate melt portion (Keays 1995). A number of processes may result in attainment of sulfur saturation. Ripley and Alawi (1988) stated that S-saturation may be attained by the introduction of S into the parent magma by devolatilization of crustal sulfides or digestion of bulk crust. The primitive REE patterns and the generally low SiO_2 contents in Gabbro Akarem rocks (El Mahallawi and Helmy 1997) indicate that there was no major crustal contamination of the Gabbro Akarem mantle magma. The S/Se ratios of the Gabbro Akarem sulfide ores are in the range of 1,890 to 4,300, which fall within the range of typical mantle-derived sulfides (Naldrett 1981a). The low As (normally <2 ppm) and Sb (<0.4 ppm) in the Gabbro Akarem rocks is consistent with an uncontaminated origin of sulfides (Barnes and Theriault 1998). The S isotope data are consistent with a magmatic origin of sulfur in Gabbro Akarem according to Sharara et al. (1999). Sulfur saturation at Gabbro Akarem magma was probably attained by simple fractionation processes (Keays 1995). The gradual increase in S content from mafic to ultramafic rocks (see Table 4) supports this inference.

Changes in the prevailing fO_2 in the melt are reflected in the ferric/ferrous iron ratios (Fe^{3+}/Fe^{2+}) in the crystallizing phases. The calculated ferric/ferrous ratio in Al–Mg-rich spinel included in olivine from the dunite pipes is in the range of 0.3–0.7, while intercumulus spinel and spinel included in sulfide have a consistently higher ratio (1.4–1.9). The wide range of spinel ferric/ferrous ratios may be related to the reaction of spinel with evolving intercumulus liquid (Roeder 1994) or subsolidus re-equilibration with olivine (Irvine 1965; Roeder 1994). The occurrence of Cr-magnetite as inclusions in sulfides and as an intercumulus phase with sulfides suggests that reaction of chrome spinel with the intercumulus liquid was not an important factor in forming the Cr-magnetite. The textural position of Cr-magnetite is more consistent with crystallization from an oxidized magma. Cr-magnetite inclusions in sulfides were probably crystallized from the sulfide melt. The textural features indicate that sulfides were precipitated after or contemporaneously with the Cr-magnetite. Coexisting spinel–orthopyroxene–olivine minerals were used to calculate the fO_2 values (Ballhaus et al. 1991). The Al–Mg-rich spinel gives low fO_2 values ($\log fO_2 = -26$ to -91) while the Cr-magnetite gives consistently high fO_2 values ranging from $\log fO_2 = -4$ to -12. These calcu-

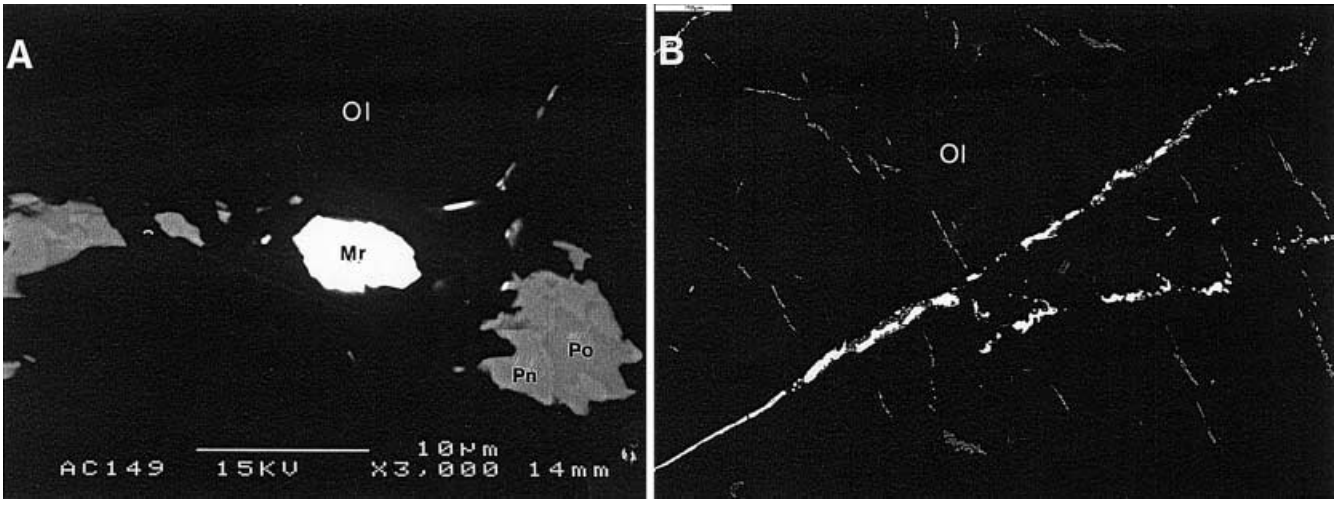

Fig. 8 **A** Merenskyite (*Mr*) with pyrrhotite (*Po*) and pentlandite (*Pn*) along crack in olivine (*Ol*), sample AC146. **B** Electrum (*white*) with magnetite (*gray*) filling cracks in olivine (*Ol*), sample GA153, *scale bar* = 50 µm

lations provide evidence on the dramatic changes in oxygen activity during the crystallization history of the Gabbro Akarem magma.

Mechanism of Cu–Ni–PGE ore formation

As a result of fractionation and accumulation of olivine and orthopyroxene, the magma became enriched in S and Cu until sulfide segregation commenced. Normally, cotectic sulfide proportions are in the range of 0.1–0.3%; however, percolation into the underlying cumulate mush (Helmy and El Mahallawi 1999) led to the observed high sulfide concentration (up to 70% in the massive ore). During uplift along the fault zone, sulfide minerals commenced crystallization, due to cooling and increase in fO_2.

Experimental studies in the Fe–Cu–S system (Craig and Kullerud 1969) and in the Fe–Ni–S system (Naldrett et al. 1967) showed that monosulfide solid solution (mss) is the first phase to crystallize during cooling. Sharara et al. (1999) suggested that pyrrhotite, pentlandite, and chalcopyrite were exsolved from mss, which is consistent with our microscopic observations. The temperature of crystallization of the lherzolites at Gabbro Akarem was estimated to be in the range of 912–888 °C (using two pyroxene geothermometry; El Mahallawi and Helmy 1997). These temperatures are considered the upper limit of sulfide separation and crystallization. Sideek and El Goresy (1996) identified troilite and monoclinic-smythite intergrowths in the Akarem sulfides. They suggested a prolonged period of equilibration to low temperatures down to 75 °C.

It is widely accepted that PGM exsolve, over a wide range of temperatures, from the sulfide liquid as it recrystallizes to different sulfides during cooling (Ballhaus and Ulmer 1995). Platinum-group minerals at Gabbro Akarem were observed either as inclusions in pyrrhotite (preferentially close to its crystal margins), at the sulfide–silicate contacts, and along cracks in olivine. Merenskyite and michenerite were probably exsolved from the sulfide liquid during cooling; merenskyite inclusions in pyrrhotite were the early formed phases while those at chalcopyrite–silicate contacts were probably formed at the last stage of sulfide crystallization. Low-temperature hydrothermal solutions may be responsible for mobilization of Pd and Au to form merenskyite and electrum in serpentine veinlets in olivine. Dominance of secondary pyrite in microfractures and the low-temperature silicate assemblage associated with merenskyite suggest that Pd was mobilized as bisulfide complexes. Experimental studies (Pan and Wood 1994) demonstrate that Pd can be transported as bisulfide complexes in fluids associated with serpentinization of sulfide-bearing ultramafic rocks.

Comparison with Cu–Ni–PGE mineralizations in other tectonic settings

In the Cu–Ni–PGE mineralization of the Salt Chuck intrusion (concentrically zoned), sulfides are dominated by bornite and chalcopyrite while PGM are represented by Pd-bismuthotellurides. As discussed above, Gabbro Akarem mineralization is dominated by pyrrhotite, pentlandite, and chalcopyrite. The absence of Ni-minerals in the Salt Chuck intrusion reflects the parent magma composition (less magnesian than that of Gabbro Akarem as indicated by the absence of olivine in the Salt Chuck intrusion, Loney and Himmelberg 1992), while the similar PGM assemblage suggests a late-magmatic hydrothermal overprint.

Although Gabbro Akarem has a sulfide mineralogy similar to other Ni–Cu–PGE deposits hosted in layered intrusions (e.g., Sudbury), it is poor in PGE and rich in S (Table 4 and Fig. 10). Barnes and Theriault (1998) discussed the relation between country-rock (sedimentary) assimilation and cooling on the one hand and the compositions of magmatic sulfides on the other hand. They concluded that the higher the volume of assimi-

Table 4 Distribution of PGE, Au, Ag, and major ore-forming elements in rocks and ore of the Gabbro Akarem Cu–Ni deposit (platinum-group elements in ppb, sulfur in wt% and others in ppm). Dunite samples represent net-textured and massive sulfide ore; *na* not analyzed

Sample no.	Rock type	S	Cu	Ni	Co	Zn	Cr	Se	Ag	Ir	Ru	Rh	Pt	Pd	Au	Os	?PGE	Ni/Cu
GA138	Plagioclase hornblendite	0.031	65	185	50	65	470	< 3	2	3	< 2	0	1	2	1	< 2	16	2.8
GA139		0.042	14	78	51	82	160	< 3	1	< 2	< 2	1	1	3	1	< 2	5	5.6
GA133		0.035	2	589	73	67	640	< 3	0	< 2	< 2	1	1	14	1	< 2	16	294
GA152	Hornblende plg pyroxenite	0.98	950	910	170	na	1600	< 3	< 0.4	< 2	< 2	< 1	51	49	790	< 2	100	0.96
GA145		1.5	1300	1100	220	18	1100	4	< 0.4	< 2	< 2	< 1	47	85	17	< 2	136	0.85
GA142		2.8	7400	1400	130	na	2300	7	< 0.4	< 2	< 2	34	20	226	1	< 2	280	0.19
GA141		2.65	9400	2750	190	na	1800	7	2	< 2	< 2	1	100	45	205	< 2	150	0.29
GA143	Olivine hbl clinopyroxenite	1.4	4370	2600	170	na	2300	3	1	< 2	< 2	< 1	92	105	63	< 2	197	0.59
GA146		1.3	2610	2100	220	48	1100	3	< 0.4	< 2	< 2	28	< 1	133	16	< 2	161	0.8
GA147		1.7	5150	3070	185	38	1850	4	< 0.4	< 2	< 2	17	35	89	56	< 2	141	0.6
GA158	Sp lherzolite	0.73	580	710	210	na	1400	< 3	< 0.4	< 2	< 2	< 1	44	48	6	< 2	92	1.22
GA159		2.8	5750	5700	320	na	870	12	1	< 2	< 2	< 1	6	10	72	< 2	16	0.99
GA163	Dunite	10.1	7500	9100	800	na	1200	24	< 0.4	< 2	< 2	26	6	123	12	< 2	165	1.21
GA153		13	11404	18000	920	140	1600	36	2	3.4	< 2	26	< 1	164	36	< 2	193.4	1.57
GA144		16	3300	1600	220	na	1000	36	< 0.4	< 2	< 2	1	79	63	57	< 2	143	0.49
GA151		14.3	9400	14000	1000	na	1600	42	< 0.4	< 2	< 2	34	1	139	34	< 2	177.6	1.49
GA157		18.4	9600	19000	1400	na	1400	39	< 0.4	< 2	< 2	25	11	230	14	< 2	266	1.98
GA155		12.5	19500	18500	1100	na	1500	28	3	20	10	18	30	160	20	5	243	0.95
GA156		11.7	13500	16050	1030	na	1350	28	3	20	6	15	40	146	15	8	235	1.19

Fig. 9 Chondrite (C1)-normalized patterns of average metal content of Gabbro Akarem rock and ore types and other PGE mineralizations in Alaskan-type complexes. Data for Salt Chuck from Loney and Himmelberg (1992) and Alaskan-type complexes (average) quoted in Louis et al. (1986). Chondrite (C1) values from Naldrett and Duke (1980)

lated sediments, the higher the cooling rate and the lower the metal content of sulfides, i.e., the more contamination, the lower the R-factor. As discussed above, crustal contamination probably was not a major process at Gabbro Akarem. It is evident that immiscible base-metal sulfides act as a collector for PGEs in magmatic systems (Naldrett and Cabri 1976). Campbell and Barnes (1984) state that sulfides which equilibrate with small reservoirs of magma become PGE-poor (low R-factor). Figure 11 illustrates the variation of total PGE and S contents for the Gabbro Akarem samples. A positive correlation between S and total PGE contents at S values of less than 3 wt% is observed but at higher S contents the content of PGE does not increase. The positive correlation of S and total PGE in the J-M Reef (Fig. 8.18 in Naldrett 1989) was taken as an indication of PGE collection by sulfides. If this concept is applied for Gabbro Akarem ore samples, sulfides acted as PGE collectors at the early magmatic stage (before final emplacement), but due to the rapid sulfide melt segregation during rapid uplift, no PGE were collected later. This can explain the low PGE contents of sulfide minerals relative to the bulk-rock levels. Therefore, the low PGE content relative to the high sulfide content of the ore is attributed to the short time the sulfides were suspended (low R-factor) in a highly dynamic environment.

Conclusions

Gabbro Akarem is one of several Precambrian concentrically zoned complexes which were intruded along deep fracture zones intersecting the Eastern Desert of Egypt in an ENE direction. Unlike other concentrically zoned complexes, the PGE mineralization at Gabbro

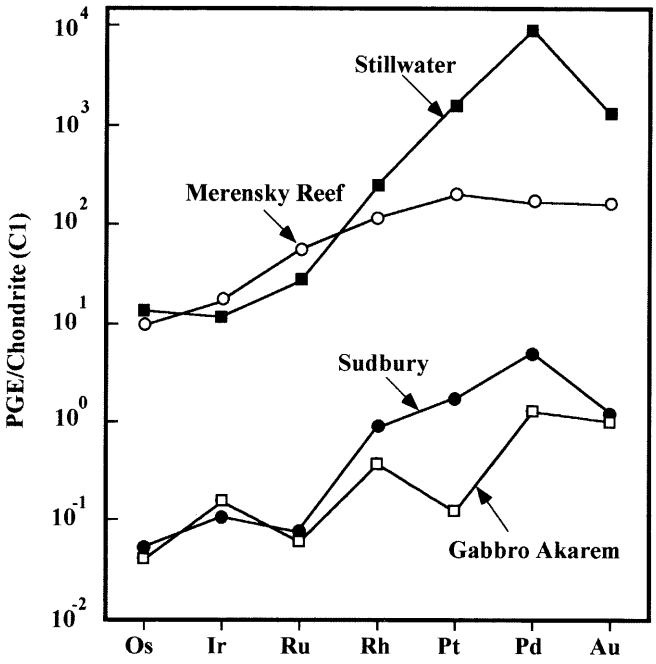

Fig. 10 Chondrite-normalized PGE patterns of massive sulfide ore from Gabbro Akarem in comparison with Merensky Reef, Stillwater, and Sudbury (data from Naldrett 1981b). PGE data are recalculated to 100% sulfides

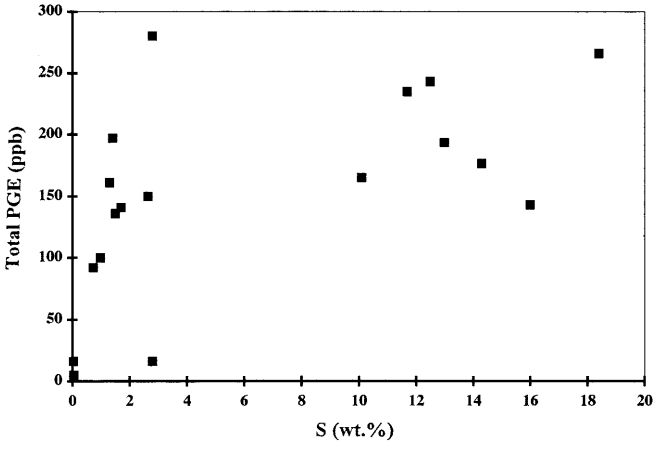

Fig. 11 Variation of total PGE versus S for the Gabbro Akarem samples

Akarem is associated with Cu–Ni ores (mainly pyrrhotite, pentlandite, and chalcopyrite) which are concentrated in the ultramafic core of the complex. Geological and geochemical evidence suggest that sulfur saturation was attained during magma fractionation and cooling where a sulfide liquid was concentrated by percolation through the cumulates to the ultramafic base of the magma chamber. Due to an abrupt increase in fO_2 and cooling during rapid uplift, sulfide minerals were crystallized from the sulfide liquid over a wide range of temperatures. Platinum-group minerals were crystallized from the sulfide melt, at high temperatures to form PGM (Pd-bismuthotellurides) inclusions in pyrrhotite and pentlandite, and at low temperatures to form PGM at sulfide–silicate interfaces. Small-scale mobilization of PGEs was effective during faulting, small-scale shearing, and serpentinization. The unique association of Cu, Ni, and PGE in this concentrically zoned complex reflects the composition of the parental magma. The rapid segregation of sulfides in a highly dynamic environment is suggested to be responsible for the generally low PGE content of the sulfide ore.

Acknowledgements The staff members of the Geological Survey of Egypt are thanked for providing drill core samples. Discussions with colleagues from the Geology Department, Minia University, I. Shalaby, Geological Survey of Egypt, and F. Melcher, Mining University, Leoben, Austria, are greatly appreciated. Comments by M.A. Takla and S. El-Gaby are gratefully acknowledged. Karl Ettinger, Institute of Mineralogy and Petrology, Karl-Franzens University of Graz, is thanked for technical help during the microprobe analytical work. We are grateful to J. Marma for reading the final manuscript and correcting the English. Comments by W.D. Maier and M. Tarkian as journal reviewers are greatly appreciated.

References

Ballhaus C, Ulmer P (1995) Platinum-group elements in the Merensky Reef: II. experimental solubilities of platinum and palladium in Fe_{1-x} S from 950 to 450 °C under controlled fS_2 and fH_2. Geochim Cosmochim Acta 59: 4881–4888

Ballhaus C, Berry RF, Green DH (1991) High pressure experimental calibration of the olivine–orthopyroxene–spinel oxygen geobarometer: implications for the oxidation state of the upper mantle. Contrib Mineral Petrol 107: 27–40

Barnes S-J, Theriault RD (1998) The influence of assimilation and cooling rate on the composition of magmatic sulphides: examples from the Muskox and Duluth intrusions. Abstr, 8th Int Platinum Symp, South Africa, p 29

Bonatti E, Hamlyn PR, Ottenello G (1981) The upper mantle beneath a young oceanic rift: peridotites from the Island of Zabargad (Red Sea). Geology 9: 474–479

Brown AV, Page NJ, Love AH (1988) Geology and platinum-group element geochemistry of the Serpentine Hill complex, Dundas Trough, western Tasmania. Can Mineral 26: 161–175

Bugrov V, Shalaby IM (1973) First discovery of Cu–Ni sulphide mineralization in gabbro–peridotite rocks in Eastern Desert of Egypt. Ann Geol Surv Egypt 3: 177–184

Cabri LJ (ed) (1981) Platinum-group elements: mineralogy, geology, recovery. CIM Spec Vol 23

Campbell IH, Barnes S-J (1984) A model of the geochemistry of the platinum-group elements in magmatic sulphide deposits. Can Mineral 22: 151–160

Carter GS (1975) Final report on the investigation of copper–nickel sulphide mineralization at Gabbro Akarem. Internal Rep, Aswan Mineral Survey Project, Geol Surv Egypt, Cairo

Chashchin VV (1998) Distinctive geochemical features of intrusions of the clinopyroxenite–wehrlite association on the Kola Peninsula. Geochem Int 36(4): 297–308

Craig JR, Kullerud G (1969) Phase relations in the Cu–Fe–Ni–S system and their application to magmatic ore deposits. In: Wilson HDB (ed) Magmatic ore deposits. Econ Geol Monogr 4: 344–357

Dixon TH (1979) Evolution of continental crust in the Late Precambrian Egyptian Shield. PhD Thesis, University of California, San Diego

Dixon TH (1981a) Gabal Dahanib, Egypt: a Late Precambrian layered sill of komatiitic composition. Contrib Mineral Petrol 76: 42–52

Dixon TH (1981b) Age and chemical characteristics of some pre-Pan-African rocks in the Egyptian Shield. Precambrian Res 14: 113–119

Efimov AA (1998) The platinum belt of the Urals: structure, petrogenesis, and correlation with platiniferous complexes of the Aldan Shield and Alaska. Abstr, 8th Int Platinum Symp, South Africa, pp 93–96

El Mahallawi MM, Helmy HM (1997) Petrology, geochemistry and petrogenesis of the Gabbro Akarem mafic–ultramafic intrusion, South Eastern Desert, Egypt. Proc 3rd Int Conf Geochem, Alexandria, Egypt, pp 87–102

Fershtater GB, Montero P, Borodina NS, Pushkarev EV, Smirnov VN, Bea F (1997) Uralian magmatism: an overview. Tectonophysics 276: 87–102

Findlay DC (1969) Origin of the Tulameen ultramafic-gabbro complex, southern British Columbia. Can J Earth Sci 6: 399–425

Garson MS, Krs M (1976) Geophysical and geological evidence of the relationship of Red Sea transverse tectonic to ancient fractures. Bull Geol Soc Am 87: 169–181

Garson MS, Shalaby IM (1976) Precambrian–Lower Paleozoic plate tectonics and metallogenesis in the Red Sea region. Geol Assoc Can Spec Pap 14: 573–596

Garuti G, Fershtater G, Bea F, Montero P, Pusharev EV, Zaccaini F (1997) Platinum-group elements as petrological indicators in mafic–ultramafic complexes of the central and southern Urals: preliminary results. Tectonophysics 276: 181–194

Hafez AMA, Abdel-Kader Z (1982) Sulphides in the Gabbro Akarem complex, South-Eastern Desert, Egypt. Proc Egypt Acad Sci XXXIV: 195–208

Hafez AMA, Abdel Kader Z, Shalaby IM (1991) Zoned mafic–ultramafic complex in Wadi Abu Hamamid, South Eastern Desert. Ann Geol Surv Egypt XVII: 53–65

Hassan MA, Hashad AH (1990) Precambrian of Egypt. In: Said R (ed) The geology of Egypt. Balkema, Rotterdam, pp 201–245

Helmy HM, ElMahallawi MM (1999) Gabbro Akarem mafic–ultramafic complex, Eastern Desert, Egypt: a Late Precambrian analog of Alaskan-type complexes. Abstr, 37th Annu Meet Egypt Geol Soc, Cairo

Helmy HM, Stumpfl EF (1995) Genesis of the Abu Swayel Cu–Ni–PGE mineralization, South Eastern Desert, Egypt. In: Pasava J, Kribek B, Zak K (eds) Mineral deposits from their origin to their environmental impacts. Balkema, Rotterdam, pp 117–120

Helmy HM, Stumpfl EF, Kamel OA (1995) Platinum-group minerals from the metamorphosed Abu Swayel Cu–Ni–PGE mineralization, South Eastern Desert, Egypt. Econ Geol 90: 2350–2360

Irvine TN (1965) Chromian spinel as petrogenetic indicator. Part 1. Theory. Can J Earth Sci 2: 648–672

Irvine TN (1967) The Duke Island ultramafic complex, southeastern Alaska. In: Wyllie PJ (ed) Ultramafic and related rocks. Wiley, New York, pp 84–97

Irvine TN (1974) Petrology of the Duke Island ultramafic complex, southeastern Alaska. Geol Soc Am Mem 138

Keays RR (1995) The role of komatiitic and picritic magmatism and S-saturation in the formation of ore deposits. Lithos 34: 1–18

Khudeir AA (1995) El Genina El Gharbia and El Genina El Sharkia ultramafic–mafic intrusions, Eastern Desert, Egypt: geology, petrology, geochemistry and petrogenesis. Bull Fac Sci Assiut Univ 24: 177–219

Khudeir AA, Abu El Rus M, Hoinkes G, Mogessie A, El Gaby S (1996) Petrogenesis of the reversely zoned Gabbro Akarem mafic–ultramafic intrusion, South Eastern Desert, Egypt. Abstr, Centenial Geol Surv Egypt, Cairo, pp 98–99

Loney RA, Himmelberg GR (1992) Petrogenesis of the Pd-rich intrusion at Salt Chuck, Prince of Wales Island: an early Paleozoic Alaskan-type ultramafic body. Can Mineral 30: 1005–1022

Louis RM, Nesbitt BE, Morton RD (1986) Geochemistry of platinum-group elements in the Tulameen ultramafic complex, southern British Columbia. Econ Geol 81: 961–973

McDonough WF, Sun S-S (1995) The composition of the earth. Chem Geol 120: 233–253

Mues-Schumacher U, Keller J, Kononova VA, Suddaby PJ (1996) Mineral chemistry and geochronology of the potassic alkaline ultramafic Inagli complex, Aldan Shield, eastern Siberia. Mineral Mag 60: 711–730

Naldrett AJ (1981a) Nickel sulphide deposits: classification, composition and genesis. Econ Geol 75th Anniv Vol: 628–685

Naldrett AJ (1981b) Platinum-group element deposits. Can Inst Min Metall, Spec Issue 23: 197–232

Naldrett AJ (1989) Stratiform PGE deposits in layered intrusions. In: Whitney JA, Naldrett AJ (eds) Ore deposition associated with magmas. Rev Econ Geol 4: 135–165

Naldrett AJ, Cabri LJ (1976) Ultramafic and related mafic rocks: their classification and genesis with special reference to the concentration of nickel sulphides and platinum-group elements. Econ Geol 71: 1131–1158

Naldrett AJ, Duke JM (1980) Platinum metals in magmatic sulphide ores. Science 208: 1417–1424

Naldrett AJ, Craig JR, Kullerud G (1967) The central portion of the Fe–Ni–S system and its bearing on pentlandite exsolution in iron–nickel sulphide ores. Econ Geol 62: 826–847

Niazy EA, Shalaby IM, Diab MB (1985) Sulphide–silicate mineral interrelations of Gabbro Akarem Ni–Cu mineralization, Eastern Desert, Egypt. Ann Geol Surv Egypt XV: 211–221

Nixon GT, Cabri LJ, Laflamme JHG (1990) Platinum-group-element mineralization in lode and placer deposits associated with the Tulameen Alaskan-type complex, British Columbia. Can Mineral 28: 503–535

Pan P, Wood SA (1994) Solubility of Pt and Pd sulphides and Au metal in aqueous bisulphide solutions. Miner Deposita 29: 373–390

Rasmy A (1982) Mineralogy of copper-nickel sulphide mineralization at Akarem area, South Eastern Desert, Egypt. Ann Geol Surv Egypt XII: 141–162

Razin LV (1976) Geologic and genetic features of forsterite dunites and their platinum-group mineralization. Econ Geol 71: 1371–1376

Ripley E, Alawi JA (1988) Sulphide mineralogy and chemical evolution of the Babbit Cu–Ni deposit, Duluth Complex, Minnesota. Can Mineral 24: 347–368

Roeder PL (1994) Chromite: from the fiery rain of chondrules to the Kilauea Iki lava lake. Can Mineral 32: 729–746

Rucklidge J (1969) Electron microprobe investigation of platinum metal minerals from Ontario. Can Mineral 9: 617–628

Shabaan MA, Hussein AA, Morsy S (1977) Geological interpretation of a magnetic survey on the Cu–Ni prospect of Gabbro Akarem, South Eastern Desert. Internal Rep, Geol Surv Egypt, Cairo

Sharara NA, Wilson GC, Rucklidge JC (1999) Platinum-group elements and gold in Cu–Ni-mineralized peridotite at Gabbro Akarem, Eastern Desert, Egypt. Can Mineral 37: 1081–1097

Sideek S, El Goresy A (1996) Phase relation of sulphide minerals at Akarem area and platinum-group minerals in chromites from Abu Seifein chromite. Abstr, Centenial Geol Surv Egypt, Cairo, pp 168–169

Snoke AW, Quick JE, Bowman HR (1981) Bear Mountain igneous complex, Klamath Mountains, California: an ultrabasic to silicic calc-alkaline suite. J Petrol 22: 501–552

Stern RJ (1981) Petrogenesis and tectonic setting of late Precambrian ensimatic volcanic rocks, central Eastern Desert of Egypt. Precambrian Res 16: 195–230

Takla MA (1971) Ore mineralogical and geochemical studies of some basic and associated ultrabasic igneous rocks, Eastern Desert, Egypt. PhD Thesis, Cairo Univ

Taylor HP Jr (1967) The zoned ultramafic complexes of southeastern Alaska: In: Wyllie PJ (ed) Ultramafic and related rocks. Wiley, New York, pp 97–121

Tistl M (1994) Geochemistry of platinum-group elements of the zoned ultramafic Alto Condoto complex, Northwest Colombia. Econ Geol 89: 158–167

Tistl M, Salazar G (1993) The magmatic evolution of northwestern South America. Zb Geol Palaeont 2(1): 439–452